Lipid Head Group Charge and Fatty Acid Configuration Dictate Liposome Mobility in Neurofilament Networks

Fabienna Arends, Himanshu Chaudhary, Paul Janmey, Mireille M. A. E. Claessens, Oliver Lieleg*

Intermediate filaments constitute a class of biopolymers whose function is still poorly understood. One example for such intermediate filaments is given by neurofilaments, large macromolecules that fill the axon of neurons. Here, reconstituted networks of purified porcine neurofilaments are studied and the diffusion behavior of different nanoparticles in the biopolymer network is evaluated. A strong dependence of particle diffusion on the charge state of the particles, and – for liposomes – also on the fatty acid configuration of lipids is observed. The results suggest that both electrostatic and hydrophobic interactions contribute to nanoparticle trapping in neurofilament networks, and that the latter is enabled by lipids with an inverted cone geometry which grant access to the hydrophobic core of the liposome shell.

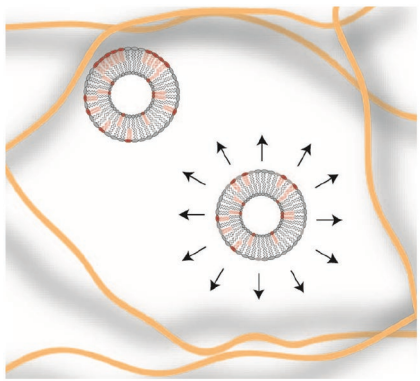

1. Introduction

Neurons are responsible for the transduction of signals and the main part of the signal transmission process takes place in the axon. At the synaptic terminus of the axon, synaptic vesicles are waiting to release their cargo, i.e., neurotransmitters, into the synaptic cleft.[1] These vesicles are assembled in the cell body and then transported along the axon to the synaptic terminus by motor proteins. During this active transport process, it is in principle possible that the vesicles unbind from the motor protein and reach the plasma membrane of the axon by diffusion. When contact between the synaptic vesicle and the plasma membrane is established this may result in fusion of synaptic vesicles with the axon membrane instead of the membrane at the synaptic cleft. In mature axons, such a fusion does not occur; it has, however, been observed in immature axons.[2,3] This indicates that there should be a mechanism in the mature axon preventing the diffusion of vesicles to the plasma membrane.

The axon of neurons is densely filled with neurofilaments, a subtype of intermediate filaments which is believed to be mostly responsible for providing mechanical support and determining the axon diameter.[4–6] However, the complex architecture of neurofilaments suggests that these biopolymers serve an additional

Dr. F. Arends, Prof. O. Lieleg
Department of Mechanical Engineering and Institute of Medical Engineering (IMETUM)
Technical University of Munich
85748, Garching, Germany
E-mail: oliver.lieleg@tum.de
Dr. H. Chaudhary, Prof. M. M. A. E. Claessens
Nanobiophysics group
MESA+ Institute for Nanotechnology and MIRA Institute for Biomedical Technology and Technical Medicine
University of Twente
7500, AE, Enschede, The Netherlands
Prof. P. Janmey
Institute for Medicine and Engineering
University of Pennsylvania
Philadelphia, PA 19104, USA

Macromol. Biosci. **2016**, DOI: 10.1002/mabi.201600229

purpose in addition to establishing mechanical stability. Neurofilaments consist of three subunits, i.e., light (NF-L), medium (NF-M), and heavy neurofilament (NF-H) subunits. All three neurofilament subunits share a common structure: a globular N-terminal head, an alpha helical part, and a C-terminal tail.[4] The three subunits mainly differ in terms of the tail length with NF-L having the shortest tail and NF-H having the longest tail domain. The three subunits assemble such that two neurofilament subunits form a coiled-coil dimer via their alpha helical domain. For this assembly step, at least one NF-L unit is required.[7] The dimers then assemble further in an antisymmetric half-staggered manner such that the tail domains extend radially at periodic distances.[8,9] The tail domains carry both negative as well as positive charges but are on average negatively charged.[10] The absolute value of this net charge depends on the degree of phosphorylation, which increases with age and also differs for neurofilaments found at different locations in the neuron: nonphosphorylated tails are mostly found in the cell body whereas, in the mature axon, they are strongly phosphorylated.[11] The presence of charged regions on the neurofilaments suggests that charge effects may be relevant for regulating the diffusion of particles as already observed in other biopolymer networks such as the basal lamina,[12–14] the vitreous humor,[15–17] and mucus.[18,19]

In general, possible interactions between particles and hydrogels comprise: geometric hindrance effects imposed by the hydrogel network, electrostatic interactions between charged particles and charged hydrogel components, and hydrophobic interactions. In the previously mentioned examples, the mesh size, which sets the length scale for geometric confinement, is on the order of several hundred nanometers.[15,17,20,21] Since biologically relevant molecules are usually much smaller than this mesh size, geometric constraints imposed by the network only play a minor role. In contrast, electrostatic interactions can trap small objects, i.e., nanoparticles or molecules.[15,17,22] The basal lamina was shown to act as an electrostatic bandpass which allows weakly charged nanoparticles to pass whereas it suppresses the diffusion of highly charged particles of either algebraic sign.[12] A similar result was obtained in native mucus and in reconstituted mucin gels: also here, both positively and negatively charged particles are immobilized.[18,23] In contrast, in the vitreous humor only positively charged particles are trapped whereas negatively charged particles can diffuse almost freely.[15,17] In addition to such charge effects, hydrophobic interactions – which are much more difficult to prove experimentally – have been put forward to contribute to the selective permeability properties of the basal lamina, mucus, and the nuclear pore complex.[14,24–26] In all three systems, key molecular motifs responsible for the trapping of charged particles have been identified. Such a detailed understanding of the physicochemical principles establishing selective permeability is, however, still missing for neurofilament networks.

Here, we demonstrate by means of single particle tracking that the diffusion of negatively as well as positively charged polystyrene particles is retarded in reconstituted neurofilament networks. When the surface of these particles is passivated by a polyethyleneglycol (PEG) layer, the particles rapidly diffuse within the gel. In contrast, when liposomes are employed as diffusion probes, we find that additional effects come into play: by varying the fatty acid configuration of the lipids used for liposome assembly, we show that the packing parameter of the lipids influences the diffusive mobility of the liposomes within the neurofilament network. We interpret these results by suggesting that certain lipid geometries grant hydrophobic neurofilament residues access to the hydrophobic core of the liposome shell. This may, in turn, enable binding of the liposomes to hydrophobic regions of the neurofilaments and thus also retard their diffusion.

2. Experimental Section

2.1. Neurofilament Purification and Quality Control

Neurofilaments were prepared from porcine spinal cords (which were obtained from a local slaughterhouse in Munich) according to the protocol of Leterrier[27] with a few adjustments to account for the different tissue source.[28] Here, the so called crude NF pellet was resuspended with a five times higher volume of reassembly buffer (RB, 0.1 M 2-(N-morpholino)ethanesulfonic acid (MES), 1×10^{-3} M (ethylene glycol-bis(β-aminoethyl ether)-N,N,N′,N′-tetraacetic acid) (EGTA), 1×10^{-3} M $MgCl_2$). After the last centrifugation step with a discontinuous sucrose gradient, the pellet was recovered with RB containing 0.8 M sucrose and dialyzed against RB + 0.8 M sucrose. After 48 h, the neurofilaments were shock frozen in liquid nitrogen and stored at −80 °C. The protein concentration was determined with a bicinchoninic acid (BCA) assay (Thermo Fisher, Braunschweig, Germany) using bovine serum albumin (BSA) as a standard.

2.2. Polystyrene Particles

Fluorescent carboxyl- and amine-terminated polystyrene latex particles with a diameter of 200 nm were obtained from Invitrogen. PEG (M_w = 750 Da, Rapp Polymere, Tübingen, Germany) coating of fluorescent 200 nm carboxyl-terminated latex beads was performed using a carbodiimide-coupling protocol.[17] Successful PEGylation was verified by determining the ζ-potential of the particles using dynamic light scattering implemented in a Zetasizer ZS (Malvern Instruments, Herrenberg, Germany): When suspended in RB + 0.8 M sucrose, a ζ-potential of $\zeta = -37$ mV for the carboxylated particles before PEGylation and $\zeta = -14$ mV after PEGylation was measured.

Macromol. Biosci. **2016**, DOI: 10.1002/mabi.201600229

2.3. Liposomes

Lipids dissolved in chloroform were obtained from Avanti Polar Lipids (Alabaster, AL, USA). Liposomes were prepared from 1,2-dioleoyl-*sn*-glycero-3-phosphocholine in either *cis* (DOPC) or *trans* configuration (tDOPC, 1,2-dioleoyl-3-trimethylammonium-propane (DOTAP), 1,2-dioleoyl-sn-glycero-3-phospho-(1′-rac-glycerol) (DOPG), 1,2-dioleoyl-*sn*-glycero-3-phosphoethanolamine-N-(lissamine rhodamine B sulfonyl) (Rh-DOPE), and L-α-phosphatidylcholine (from porcine brain, POPC). Lipids were mixed in the desired ratio to a total amount of 0.3 μmol, and solvent evaporation was conducted over night. Dried lipids were resuspended with 0.5 mL RB containing 0.8 M sucrose, then vortexed and sonicated for several minutes. Afterward, the size of the liposomes was adjusted to 200 nm by extrusion with a mini extruder (Avanti Polar Lipids, AL, USA). The ζ-potential of the liposomes was measured with the Zetasizer ZS (Malvern Instruments, Herrenberg, Germany).

2.4. Giant Unilamellar Vesicles

Giant unilamellar vesicles (GUVs) were prepared from 10 mg mL^{-1} stock solutions of POPC, 1-palmitoyl-2-oleoyl-*sn*-glycero-3-phospho (1′-rac-glycerol), DOPC, DOPG, and a 0.1 mg mL^{-1} stock solution of Rh-DOPE in chloroform. The lipid solutions were mixed at different ratios. One mol% of Rh-DOPE was included in the lipid mixtures to allow visualization of the GUVs in confocal microscopy experiments. To prevent saturation of the lipid fluorescence, the Rh-DOPE content of the GUVs was limited to 1 mol%. GUVs were prepared by the electroformation method as described before.[29] The lipids suspended in chloroform were deposited drop by drop onto a custom-built platinum (Pt) wire electrode with a diameter of 0.762 mm. The deposited lipids were dried using a nitrogen stream. After drying of the lipids, the electrodes were transferred to a cuvette filled with 1 mL of RB, containing 0.8 M sucrose, and connected to a frequency generator (PCGUI 1000 Velleman). Electro-swelling was conducted at 500 Hz at room temperature, and during detachment of vesicles the frequency was gradually decreased from 500 to 50 Hz.[30]

2.5. Diffusion Experiments

For diffusion experiments, neurofilaments were thawed on ice for several hours and used at a protein concentration of 1 mg mL^{-1}. Gelation was induced in presence of the respective test particles at room temperature for 24 h. Particle tracking experiments were conducted on an Axiovert 200 (Zeiss, Oberkochen, Germany) microscope with a 40× objective (Zeiss, Oberkochen, Germany). Movies for single particle tracking were acquired with a digital camera (Orca Flash 4.0 C11440, Hamamatsu, Japan) using the software Hokawo provided by Hamamatsu. The length of the videos was 5 s and the frame rate was 100 s^{-1}, which resulted in 500 images per movie. Particle trajectories were obtained and analyzed as described previously.[14] In brief, the particle position was determined for each frame by fitting a Gaussian to the x- and y-section of the intensity profile of each particle. From the trajectory $\vec{r}(t)$ of a particle, the mean-square displacement (MSD) was then determined according to

$$\mathrm{MSD}(\tau) = \frac{1}{N}\sum_{i=1}^{N}\left[\vec{r}(i\Delta t+\tau)-\vec{r}(i\Delta t)\right]^2 \quad (1)$$

To avoid artifacts arising from statistical limitations, an apparent diffusion coefficient via $\mathrm{MSD}(\tau)=4D\tau$ was calculated only from the first 10% of the MSD data which corresponds to $\tau = 500$ ms (see also Figure S1, Supporting Information). On this short time scale, geometric hindrance effects such as caging should not play a role. Thus, low apparent diffusion coefficients are attributed to binding of particles to the neurofilaments. In every sample, particles from at least three different fields of view were analyzed. Thus, a total of at least 1000 particles were analyzed for each particle species.

2.6. Confocal Microscopy

After ≈30 min of incubation with a 250×10^{-9} M neurofilament solution at room temperature, GUVs were visualized on a Zeiss confocal laser scanning microscope (CLSM) using 63× Plan-Apochromat 1.4 NA oil immersion objective. The Rh-DOPE fluorescence from the GUVs was excited at 543 nm using a green helium neon laser. The fluorescent signals from Rh-DOPE were acquired using the appropriate dichroic mirrors. The images were then processed with the software Zen lite 2012.

3. Results and Discussion

We here conduct diffusion studies in reconstituted neurofilament networks. Our purification process yields a comparable protein mixture (Figure S2, Supporting Information) as described in the literature.[28,31] When polystyrene particles are embedded into such a neurofilament network, both negatively (COOH-terminated) and positively (NH_2-terminated) charged beads show retarded diffusion with an average apparent diffusion coefficient of $\langle D\rangle_{COOH} = 0.06$ μm^2 s^{-1} and $\langle D\rangle_{NH2} = 0.12$ μm^2 s^{-1}, respectively (Figure 1A). In contrast, when the surface of the polystyrene particles is passivated by PEGylation, the distribution of particle diffusion coefficients is shifted to larger values, and we obtain an approximately tenfold higher average diffusion coefficient of $\langle D\rangle_{PEG} = 0.97$ μm^2 s^{-1}.

This value determined for the PEGylated particles is only twofold smaller than the theoretical diffusion coefficient for unrestricted Brownian motion of 200 nm particles in water. This result suggests that this particle species can almost freely diffuse within the neurofilament network and that the chosen tracer particles are smaller than the mesh-size of the neurofilament network (Figure S3, Supporting Information). For the remainder of this article, we distinguish "immobile" ($D < D_{limit} = 0.1$ μm^2 s^{-1}) from "mobile" particles ($D \geq D_{limit} = 0.1$ μm^2 s^{-1}), similar to our previous study on particle diffusion in basal lamina gels.[14] The threshold value D_{limit} denotes 10% of the average diffusion coefficient obtained for PEGylated particles.

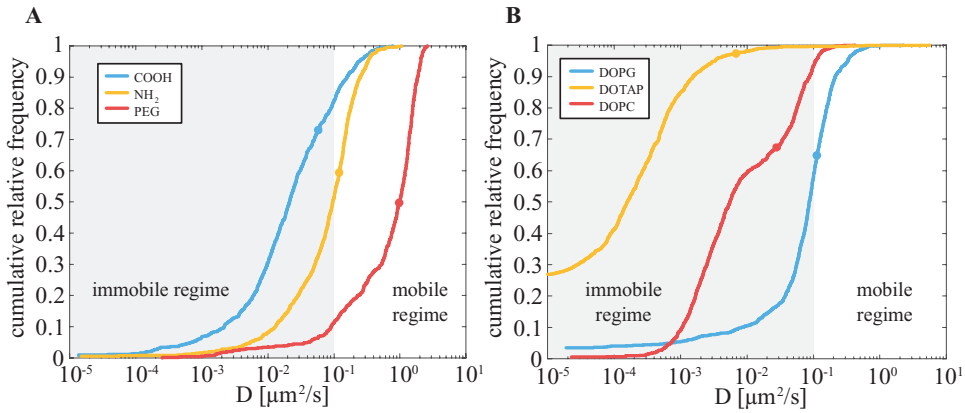

Figure 1. The mobility of polystyrene particles and liposomes in neurofilament networks depends on the particle surface properties. A) Negatively charged (COOH) and positively charged (NH_2) polystyrene particles show a low average diffusion coefficient (blue and orange dot) compared to passivated particles (PEG) which show a high diffusion coefficient (red dot). B) For negatively (DOPG) and positively (DOTAP) charged liposomes slowed-down diffusion is obtained as well (blue and orange dot). Surprisingly, also weakly charged DOPC liposomes show retarded diffusion (red dot). Similar to our previous study,[14] the boundary separating the "immobile" from the "mobile" particle regime is chosen at D_{limit} = 0.1 μm² s^{-1}. This threshold value denotes 10% of $\langle D \rangle_{PEG}$.

The observed difference in the diffusive mobility of the different particle species might be a result of electrostatic interactions between the particles and the surrounding neurofilament network as already observed for many other biological hydrogels such as the basal lamina,[12,14,22] mucus/mucin gels,[18,19,25] and the vitreous humor.[15,17] Neurofilaments are bottlebrush-like filaments with highly charged side arms extending radially from the neurofilament backbone.[8] Depending on the degree of phosphorylation, the net charge of the neurofilaments varies from almost neutral (i.e., at low degree of phosphorylation) to highly negative (i.e., at high degree of phosphorylation). Thus, electrostatic interactions with positively charged polystyrene particles might be responsible for the observed retardation of the positively charged amine-particles. However, neurofilaments side arms are not homogeneously charged, they also carry positively charged blocks.[10] Thus, in a neurofilament network, both highly negatively charged as well as highly positively charged areas are present which, in turn, allows the neurofilaments to interact with both positively and the negatively charged particles through electrostatic forces. It has been shown in several other biological hydrogel systems that such electrostatic interactions can be efficiently reduced by PEGylating the particles.[32] This notion is supported by the ζ-potential values determined for the three polystyrene particle species used here (Table 1).

In a next set of experiments, liposomes are used since those particles are biologically relevant and possess a hydrophilic surface that can additionally carry charges. One key advantage of liposomes over polystyrene particles is that the net charge of liposomes can be tuned by adjusting the lipid mixture used for liposome generation. The results obtained for negatively (DOPG) and positively (DOTAP) charged liposomes are in good agreement with the results obtained for polystyrene particles: DOPG and DOTAP liposomes both show retarded diffusion with an average diffusion coefficient of $\langle D \rangle_{DOPG}$ = 0.11 μm² s^{-1} and $\langle D \rangle_{DOTAP}$ = 0.006 μm² s^{-1}, respectively (Figure 1B). This result agrees with the data obtained for COOH- and NH_2-terminated polystyrene particles considering that the DOPG and DOTAP liposomes have high ζ-potentials. When liposomes are assembled from the zwitterionic lipid DOPC, we measure a ζ-potential that is even closer to zero than that of the PEGylated polystyrene particles discussed before (Table 1). Thus, one would expect those liposomes to be at least as mobile as the PEGylated tracer particles. However, we observe the opposite and measure an average diffusion coefficient $\langle D \rangle_{DOPC}$ = 0.03 μm² s^{-1} which is similarly low as the value obtained

Table 1. ζ-potential of polystyrene particles and liposomes.

Particle/liposome type	ζ [mV]
COOH-polystyrene particle	−37
PEG-polystyrene particle	−14
NH_2-polystyrene particle	+6
95% DOPG + 5% Rh-DOPE	−41
95% DOPC + 5% Rh-DOPE	−9
95% DOTAP + 5% Rh-DOPE	+27
95% POPC + 5% Rh-DOPE	−9
90% POPC + 10% Rh-DOPE	−15
90% POPC + 5% DOPG + 5% Rh-DOPE	−15
95% tDOPC + 5% Rh-DOPE	−9
90% tDOPC + 10% Rh-DOPE	−15

Macromolecular Journals

Macromol. Biosci. **2016**, DOI: 10.1002/mabi.201600229

for the two strongly charged liposome variants (Figure 1B). This result seems to challenge our previous assumption that electrostatic interactions are responsible for the retarded diffusion of tracer particles. However, the DOPC liposomes have a slightly negative ζ-potential; in part, this is due to the fluorescently labeled lipid rhodamine-DOPE (Rh-DOPE), which is negatively charged and present in all liposomes at a content of 5 mol%. This negative charge on the liposome surface might therefore interact with the charged neurofilaments. However, 5 mol% Rh-DOPE only introduces a very low amount of charge on the liposome surface. In synaptic vesicles, typically an even higher concentration of charged lipids of 10%–20% is incorporated.[33,34] Another key difference from the artificial liposomes used here (which are assembled from DOPC) is that the main lipid present in synaptic vesicles is POPC. When we assemble liposomes from POPC lipids, the resulting ζ-potential is –9 mV (Table 1) and thus equal to the ζ-potential of the DOPC liposomes. However, the POPC liposomes are mobile and exhibit an average diffusion coefficient of $\langle D \rangle_{POPC} = 0.97\ \mu m^2\ s^{-1}$ (Figure 2) which is similarly high as the value determined for the PEGylated polystyrene particles (Figure 1A).

In contrast to the PEGylated particles we observe a plateau for the POPC liposomes between a diffusion coefficient of $D = 0.1\ \mu m^2\ s^{-1}$ and $D = 0.4\ \mu m^2\ s^{-1}$. In other words, for POPC liposomes we find two subpopulations with clearly different behavior: diffusing particles and trapped particles. These differences in the liposome mobility may result from slight differences in the lipid composition within a given liposome preparation batch as described previously.[12] Also for the PEGylated particles (Figure 1A) and the DOPC liposomes (Figure 1B), the diffusion behavior is slightly heterogeneous. The lower diffusion coefficients measured for the PEGylated particles might be due to incomplete PEGylation as indicated by the slightly negative ζ-potential (Table 1). Such incomplete PEGylation can, in turn, give rise to a sticky diffusion process as it was observed for particle diffusion in basal lamina gels.[14] For the DOPC liposomes, we speculate that slight variations in the Rh-DOPE content give rise to both weakly and strongly bound liposome particles. This idea would agree with the result that the corresponding apparent diffusion coefficient values are heterogeneous but all lower than the "mobility" threshold defined before.

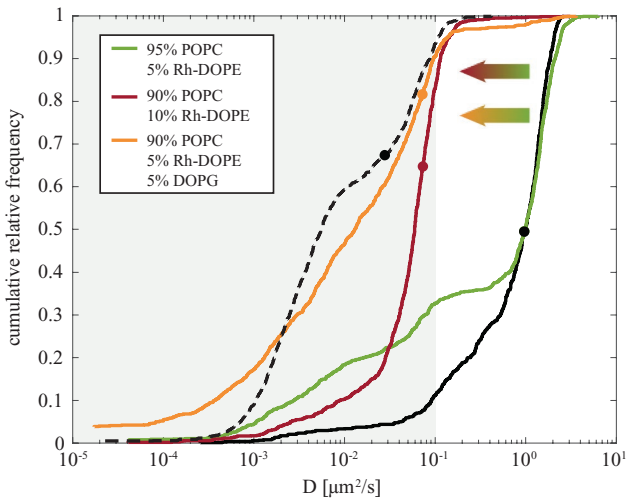

Figure 2. Cumulative distribution of diffusion coefficients of liposomes. When liposomes are assembled from POPC (green line) instead of DOPC (black dashed line) a similar diffusion coefficient as for passivated polystyrene particles (black solid line) is obtained. When the concentration of charged fluorophore on the liposome surface is increased (90% POPC + 10% Rh-DOPE, red line), the diffusion coefficient decreases. The same low diffusion coefficient is obtained for liposomes comprising 90% POPC, 5% DOPG, and 5% Rh-DOPE (orange dot).

As slight variations in the lipid composition seem to be sufficient to significantly alter the diffusion behavior of liposomes, we next ask if a small increase in the surface charge density of the liposome particles can suppress their mobility. As described before, a fraction of 5 mol% of charged lipids is not sufficient to retard the diffusive mobility of POPC liposomes. However, when we increase the concentration of negatively charged Rh-DOPE in the POPC liposomes to 10 mol%, the distribution of diffusion coefficients is shifted towards lower values (Figure 2). The calculated average diffusion coefficient of $\langle D \rangle_{POPC,10} = 0.07\ \mu m^2\ s^{-1}$ is similar to the value determined for DOPC liposomes. This indicates that, also for the POPC liposomes, there is a charge threshold above which the liposome particles become immobilized. The almost identical result is obtained when POPC liposomes are assembled with 5 mol% Rh-DOPE and 5 mol% DOPG (Figure 1), i.e., when part of the surface charge is established by DOPG instead of Rh-DOPE. This demonstrates that the observed liposome trapping effect is not specific with respect to the chemical origin of the negative surface charge.

Why is the diffusive mobility of DOPC liposomes and POPC liposomes different even though their ζ-potentials are identical? Since DOPC and POPC have the same phosphocholine head domain, liposomes assembled from those two lipid variants should have the same surface properties. However, POPC carries one palmitic acid chain instead of oleic acid; as a consequence, the two lipids differ in terms of their geometry: This geometry of lipids can be quantified by the packing parameter (PP) which compares the actual volume of a lipid to that of a cylinder of similar dimensions.[35] A PP value close to 1 is obtained for cylindrical lipids, PP values significantly larger than 1 indicate an inverted cone geometry whereas small PP values are found for conical lipids. For DOPC, this packing parameter is $PP_{DOPC} = 1.08$[36] whereas POPC has a packing

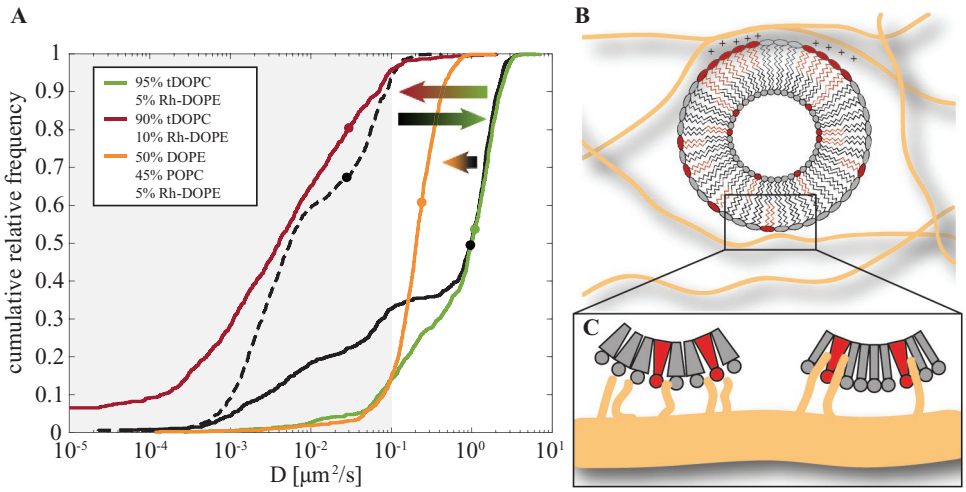

Figure 3. The configuration of fatty acids affects liposome mobility. A) Liposomes assembled from trans-DOPC (green line) show a higher diffusion coefficient than liposomes assembled from *cis*-DOPC (black dashed line). The black solid line represents the data obtained for POPC liposomes as reference. Increasing the amount of Rh-DOPE to 10 mol% (red line) decreases the diffusion coefficient. Alternatively, the mobility of the liposome population can also be retarded by increasing the DOPE content (orange line). B,C) Schematic illustration depicting two possible mechanisms which might be responsible for the retardation of liposome diffusion. B) The formation of local clusters of charged lipids or C) lipid-dependent access to the hydrophobic core of the liposome shell are two conceivable scenarios which could induce binding of liposomes to the neurofilaments (see main text for details).

parameter of $PP_{POPC} = 0.65$.[37] Thus, DOPC is best approximated by a cylindrical shape, and POPC is described best by a cone geometry. If the packing parameter of the lipids is indeed responsible for the observed difference in liposome mobility, then replacing DOPC by another lipid variant with a smaller packing parameter should also lead to mobile liposomes. To test this hypothesis, we assemble liposomes from DOPC lipids which carry oleic acid chains in *trans* configuration (tDOPC) instead of the *cis*-DOPC molecules used so far. As those two lipids, tDOPC and DOPC, are chemically very similar, they should possess identical electrochemical properties but tDOPC should have a smaller packing parameter. Indeed, when we perform diffusion experiments with liposomes assembled from tDOPC, we obtain an average diffusion coefficient of $\langle D \rangle_{tDOPC} = 1.1\ \mu m^2\ s^{-1}$ (Figure 3A) which is similarly high as the value obtained for PEGylated particles. This underscores our previous notion that the geometry of the lipids affects the diffusive mobility of liposomes in a neurofilament network.

When the amount of charge on the surface of those tDOPC liposomes is increased by incorporating 10 mol% Rh-DOPE lipids, the ensemble diffusion coefficient drops again: we now determine a value of $\langle D \rangle_{tDOPC,10} = 0.03\ \mu m^2\ s^{-1}$, which is similarly low as the value obtained for *cis*-DOPC liposomes. Thus, we are able to mobilize DOPC liposomes by changing the geometry of the DOPC lipids, and we can immobilize the latter liposomes again by increasing the surface charge density on the liposome shell.

From the data presented so far, we can conclude that there must be a charge cut-off value above which liposomes become restricted in their diffusive mobility. However, liposomes with identical ζ-potentials can behave differently when the lipids they are assembled from have different geometries. As mentioned previously, the Rh-DOPE lipids add charges to the liposome surface, but the Rh-DOPE lipids should be statistically distributed across the whole liposome shell. Since the lipids are not spatially fixed, they should be able to laterally diffuse within the bilayer. Thus, it might be possible that the charged Rh-DOPE lipids form patches when the liposomes are in close proximity to the charged neurofilaments. Those lipid patches could then bind to the neurofilaments via electrostatic interactions which might explain the observed liposome trapping (Figure 3B). In such a scenario, the POPC lipids could reduce the lateral mobility of the charged Rh-DOPE lipids, which in turn would hamper the charge-induced phase separation of the lipids. Then, higher concentrations of charged lipids would be required to induce liposome arrest.

If this mechanism indeed occurs, then we should be able to visualize this local enrichment of Rh-DOPE. For this purpose, we prepared GUVs and incubated them with a neurofilament solution. Neither in POPC nor in DOPC GUVs containing 5 mol% negatively charged lipids any sign of the formation of Rh-DOPE rich patches was observed at the length scales visible in fluorescence microscopy experiments (Figure 4; Figure S4, Supporting Information). The variation of the Rh-DOPE fluorescence intensity around the vesicle contour in the equatorial plane does not result from domain formation but reflects the orientation of the Rh-DOPE in the

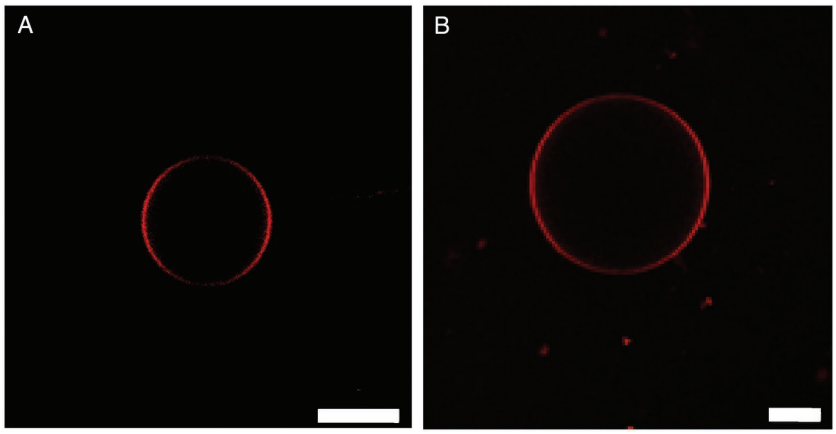

Figure 4. Visualization of Rh-DOPE distribution in GUVs in the presence of neurofilaments. A) When a 250×10^{-9} M neurofilament solution is incubated with POPC:DOPG:Rh-DOPE (95:4:1) GUVs or B) DOPC:DOPG:Rh-DOPE (95:4:1) GUVs, the Rh-DOPE fluorescence remains homogeneous. There is no sign of enrichment of Rh-DOPE in macroscopically visible patches. The scale bars represent 10 µm.

membrane with respect to the axis of polarized excitation light.[38]

Since we did not observe a neurofilament-induced local enrichment of Rh-DOPE, there has to be another mechanism responsible for retarding liposome diffusion. The data presented so far strongly suggests that the geometry of the lipids somehow contributes to the immobilization of liposomes. For the interaction of vesicles with monomers and oligomers of the protein alpha-synuclein it was observed that a combination of electrostatic and hydrophobic forces conveys membrane binding.[39,40] A similar process might also occur in the liposome-neurofilament system. Indeed, the side arms of the neurofilaments are not only charged but also carry hydrophobic amino acids which constitute 20% of the peptide sequence (averaged over the three subunits). Thus, hydrophobic interactions between the neurofilaments and the liposomes are theoretically possible provided that the hydrophobic core of the lipid shell is accessible to the neurofilaments (Figure 3C). Since DOPE is shaped like an inverted truncated cone, i.e., its head group is smaller in diameter than the cross-section of volume filled by the fatty acids (resulting in a large packing parameter of $PP_{DOPE} = 1.34$[37]), the hydrophobic part of the bilayer might indeed be accessible from the outside of the liposome. In turn, when POPC is used instead of DOPC, the conical shape of the POPC lipids might prevent neurofilaments from accessing the hydrophobic regions of DOPE lipids by filling the gaps in the outer surface of the liposome shell. So far, this model – even though speculative – would be consistent with the data presented. To challenge our model, we ask if POPC-based liposomes may be rendered immobile by increasing the accessibility of the hydrophobic lipid parts. Experimentally, this should be possible by introducing a higher amount of DOPE lipids into the liposome shell. However, to clearly disentangle the contribution of hydrophobic interactions with that of electrical forces, it is important not to introduce additional charges into the liposome surface as well. Thus, unlabeled DOPE lipids are added for this experiment. As depicted in Figure 3A, liposomes comprising 50 mol% DOPE, 45 mol% POPC, and 5 mol% Rh-DOPE are indeed slowed down ($\langle D \rangle = 0.23$ µm^2 s^{-1}) compared to the mobile POPC/Rh-DOPE liposomes. However, this ensemble diffusion coefficient is still higher than that observed for DOPC/Rh-DOPE liposomes; our explanation does not yet capture all features of this complex system.

4. Conclusion

Due to their structural complexity, the range of interactions possible between liposomes and biopolymer hydrogels such as neurofilament networks are quite complex: Electrostatic interactions of neurofilaments with the membrane may result in the formation of domains rich in charged lipids. Moreover, in addition to charge interactions, also hydrophobic interactions appear to play a role in the system studied here. Our results suggest that certain lipid geometries grant access to the hydrophobic core of the liposome shell, which in turn enables binding of the liposomes to hydrophobic regions of the neurofilaments. Such a combination of electrostatic interactions and hydrophobic forces has already been observed for the binding of synaptotagmin I to phospholipid bilayers[41] and for the binding of model peptides to liposomes.[42] Our results motivate that a similar mechanism as described here may also prevent free synaptic vesicles, i.e., those which have unbound from the motor protein during their transport along the axon, from fusing with the plasma membrane of the axon. Of course, in synaptic vesicles, the vesicle surface is in part covered by proteins, which may introduce additional interactions with the neurofilament network – or weaken those established by the lipid shell. However, the composition of vesicles is thought to become more complex during their transport along the axon[1] which could be another factor affecting the mobility of those vesicles in neurons. Thus, the in vitro results described here can, of course, not directly explain the complex behavior of synaptic vesicles in vivo. They do, however, show that a combination of different physical mechanisms needs to be considered when discussing the diffusion behavior of

multi-component particles such as liposomes in complex biological environments such as neurofilament networks.

Supporting Information

Supporting Information is available from the Wiley Online Library or from the author.

Acknowledgements: The authors thank Jan Lang for performing pilot experiments for this study and Angela Otto for helpful discussions. This project was supported by the Deutsche Forschungsgemeinschaft (DFG) through Grant No. LI-1902/3-1. MMAEC and HC acknowledge support from the NWO-CW VIDI (Grant No. 700.59.423).

Received: June 3, 2016; Revised: August 9, 2016; Published online: ; DOI: 10.1002/mabi.201600229

Keywords: axon; diffusion; intermediate filaments; vesicles

[1] S. O. Rizzoli, *EMBO J.* **2014**, *33*, 788.
[2] L. Polo-Parada, C. M. Bose, L. T. Landmesser, *Neuron* **2001**, *32*, 815.
[3] T. A. Ryan, *Neuron* **2001**, *32*, 759.
[4] A. D. Yuan, M. V. Rao, Veeranna, R. A. Nixon, *J. Cell Sci.* **2012**, *125*, 3257.
[5] R. L. Friede, T. Samorajs, *Anat. Rec.* **1970**, *167*, 379.
[6] W. C. Lin, B. G. Szaro, *J. Neurosci.* **1995**, *15*, 8331.
[7] J. A. Cohlberg, H. Hajarian, T. Tran, P. Alipourjeddi, A. Noveen, *J. Biol. Chem.* **1995**, *270*, 9334.
[8] R. Beck, J. Deek, J. B. Jones, C. R. Safinya, *Nat. Mater.* **2010**, *9*, 40.
[9] J. Liu, X. J. Tong, S. J. Pang, Z. H. Zhai, *Appl. Surf. Sci.* **1999**, *144–45*, 644.
[10] J. B. Jones, C. R. Safinya, *Biophys. J.* **2008**, *95*, 823.
[11] J. Brownlees, A. Yates, N. P. Bajaj, D. Davis, B. H. Anderton, P. N. Leigh, C. E. Shaw, C. C. J. Miller, *J. Cell Sci.* **2000**, *113*, 401.
[12] O. Lieleg, R. M. Baumgärtel, A. R. Bausch, *Biophys. J.* **2009**, *97*, 1569.
[13] D. Vllasaliu, F. H. Falcone, S. Stolnik, M. Garnett, *Exp. Cell Res.* **2014**, *323*, 218.
[14] F. Arends, R. Baumgärtel, O. Lieleg, *Langmuir* **2013**, *29*, 15965.
[15] Q. G. Xu, N. J. Boylan, J. S. Suk, Y. Y. Wang, E. A. Nance, J. C. Yang, P. J. McDonnell, R. A. Cone, E. J. Duh, J. Hanes, *J. Controlled Release* **2013**, *167*, 76.
[16] T. F. Martens, D. Vercauteren, K. Forier, H. Deschout, K. Remaut, R. Paesen, M. Ameloot, J. F. J. Engbersen, J. Demeester, S. C. DeSmedt, K. Braeckmans, *Nanomedicine* **2013**, *8*, 1955.
[17] B. T. Käsdorf, F. Arends, O. Lieleg, *Biophys. J.* **2015**, *109*, 2171.
[18] S. K. Lai, D. E. O'Hanlon, S. Harrold, S. T. Man, Y. Y. Wang, R. Cone, J. Hanes, *Proc. Natl. Acad. Sci. USA* **2007**, *104*, 1482.
[19] Y. Cu, W. M. Saltzman, *Mol. Pharmaceutics* **2009**, *6*, 173.
[20] S. K. Lai, Y. Y. Wang, K. Hida, R. Cone, J. Hanes, *Proc. Natl. Acad. Sci. USA* **2010**, *107*, 598.
[21] F. Arends, C. Nowald, K. Pflieger, K. Boettcher, S. Zahler, O. Lieleg, *PLoS One* **2015**, *10*, e0118090.
[22] F. Arends, S. Sellner, P. Seifert, U. Gerland, M. Rehberg, O. Lieleg, *Lab Chip* **2015**, *13*, 3326.
[23] O. Lieleg, I. Vladescu, K. Ribbeck, *Biophys. J.* **2010**, *98*, 1782.
[24] Y. Y. Wang, S. K. Lai, C. So, C. Schneider, R. Cone, J. Hanes, *PLoS One* **2011**, *6*, e21547.
[25] H. M. Yildiz, L. Speciner, C. Ozdemir, D. E. Cohen, R. L. Carrier, *Biomaterials* **2015**, *54*, 1.
[26] K. Ribbeck, D. Gorlich, *EMBO J.* **2002**, *21*, 2664.
[27] J. F. Leterrier, J. Käs, J. Hartwig, R. Vegners, P. A. Janmey, *J. Biol. Chem.* **1996**, *271*, 15687.
[28] S. Rammensee, P. A. Janmey, A. R. Bausch, *Eur. Biophys. J. Biophy.* **2007**, *36*, 661.
[29] H. Chaudhary, A. N. D. Stefanovic, V. Subramaniam, M. M. A. E. Claessens, *FEBS Lett.* **2014**, *588*, 4457.
[30] T. Pott, H. Bouvrais, P. Meleard, *Chem. Phys. Lipids* **2008**, *154*, 115.
[31] J. F. Leterrier, P. A. Janmey, J. Eyer, *Biochem. Biophys. Res. Commun.* **2009**, *384*, 37.
[32] O. Lieleg, K. Ribbeck, *Trends Cell Biol.* **2011**, *21*, 543.
[33] A. Nagy, R. R. Baker, S. J. Morris, V. P. Whittaker, *Brain Res.* **1976**, *109*, 285.
[34] E. W. Westhead, *Ann. N. Y. Acad. Sci.* **1987**, *493*, 92.
[35] J. N. Israelachvili, D. J. Mitchell, B. W. Ninham, *J. Chem. Soc. Faraday Trans. 2* **1976**, *72*, 1525.
[36] D. Marsh, *Biophys. J.* **1996**, *70*, 2248.
[37] G. Lantzsch, H. Binder, H. Heerklotz, M. Wendling, G. Klose, *Biophys. Chem.* **1996**, *58*, 289.
[38] C. K. Haluska, A. P. Schroder, P. Didier, D. Heissler, G. Duportail, Y. Mely, C. M. Marques, *Biophys. J.* **2008**, *95*, 5737.
[39] M. Stockl, P. Fischer, E. Wanker, A. Herrmann, *J. Mol. Biol.* **2008**, *375*, 1394.
[40] B. D. vanRooijen, M. M. A. E. Claessens, V. Subramaniam, *Biochim. Biophys. Acta Biomembr.* **2009**, *1788*, 1271.
[41] S. H. Gerber, J. Rizo, T. C. Sudhof, *Diabetes* **2002**, *51*, S12.
[42] M. Dathe, M. Schumann, T. Wieprecht, A. Winkler, M. Beyermann, E. Krause, K. Matsuzaki, O. Murase, M. Bienert, *Biochemistry* **1996**, *35*, 12612.